

Convergence analysis of a multigrid algorithm for the acoustic single layer equation

S.Gemrich*, J.Gopalakrishnan† N.Nigam‡

September 7, 2018

Abstract

We present and analyze a multigrid algorithm for the acoustic single layer equation in two dimensions. The boundary element formulation of the equation is based on piecewise constant test functions and we make use of a weak inner product in the multigrid scheme as proposed in [4]. A full error analysis of the algorithm is presented. We also conduct a numerical study of the effect of the weak inner product on the oscillatory behavior of the eigenfunctions for the Laplace single layer operator.

This paper is dedicated to Prof. G.C.Hsiao on the occasion of his 75th birthday.

1 Introduction

A model for the scattering of acoustic waves by a bounded obstacle is given by the Helmholtz equation in the exterior of the scatterer, with appropriate growth conditions on the scattered field. One can reformulate this problem in terms of integral equations on the surface of the scattering object via direct or indirect boundary integral formulations. Or one may consider scattering from a coated bounded obstacle, in which case an integral equation can be used to prescribe a non-reflecting condition on an artificial surface surrounding the object. In both, one has to find numerical approximations to solutions of boundary integral equations. In this context, Galerkin type methods have been studied extensively and become popular over recent years, see for example the monographs [23], [16].

Our focus in this paper lies on integral equations of the first kind, which arise naturally in the direct boundary integral method for the Dirichlet problem. The main integral operator involved is called the single layer operator and may be viewed as a pseudo-differential operator of order minus one. Several authors have observed advantages of using integral equations of the first kind (e.g. [17]),

*Dept. of Mathematics and Statistics, McGill University

†Dept. of Mathematics, Portland State University

‡Dept. of Mathematics and Statistics, McGill University

for example when the scattering object is very thin (e.g. [15]) or when the scattering surface is not smooth. Indeed, for problems of crack propagation in elasticity or scattering from a screen, integral equations of the first kind are the most appropriate model.

Other popular integral equation strategies include the use of combinations of single and double layer operators, to avoid issues of non-uniqueness and the potential for numerical instability near possible eigenvalues of the operators. These approaches include the famous Brakhage-Werner and Burton-Miller formulations. In these cases as well, discrete strategies rely on effective and accurate approximation methods for the layer operators involved.

Due to the non-local behavior of boundary integral operators, they typically lead to dense linear systems upon discretization. Though one only needs to mesh on a surface of co-dimension one, the fill-in in the matrices corresponding to the integral operators is significant. Without some form of preconditioning or acceleration, these methods then become prohibitive.

One possible preconditioning strategy is the use of a multigrid scheme. However, the use of standard multigrid smoothing operations is inappropriate for negative order pseudodifferential operators. Such operators link highly oscillatory eigenfunctions to small magnitude eigenvalues. This ruins the basic interplay between standard smoothing of oscillatory error components and the possibility to represent the remaining error components on coarser grids. The remedy for this is the use of a weaker inner product in order to modify this spectral feature of the operator. This approach has first been described in [4] for positive-definite operators. We follow the same path for the acoustic single layer equation. The numerical examples in Section 4 exemplify how the spectral behavior of the discretized operators changes through the use of the weaker inner products.

Several related works can be found in the literature. The single layer equation associated to Laplace's equation has been treated and analyzed in [12] using a BPX preconditioner. The same equation was considered in [19]. Here, the authors studied a multigrid method for large-scale data-sparse approximations to the single layer operator. In the acoustics case, the use of Haar basis functions and compression type multilevel algorithms for integral equations of the first kind has been studied in [21]. Algebraic multigrid preconditioners, based on the smoother in [4], have been developed in [18].

The purpose of this paper is to prove convergence of the multigrid algorithm given in [4] when applied to the indefinite acoustic single layer discretization. We will make use of perturbation-type arguments such as in [3] and [14]. We also state the algorithm in the situation where a non-uniform discretization is used.

The design of the algorithm heavily relies on the above references and we have reported its promising numerical performance in [13]. Currently, our codes assemble and multiply matrices in $O(n^2)$ complexity, and so the computational cost of the iterative solution by multigrid is the same. The efficient assembly and matrix multiplication of the corresponding matrices is an active research issue in multipole and hierarchical matrix theories. Our numerical results indicate that

we can approach optimality in complexity through multigrid, once assembly and matrix multiplications are done optimally.

At this juncture, we note important directions for extending this work, motivated by recent developments in the study of boundary integral equation methods. Firstly, the use of combined integral equation formulations, including those by Brakhage-Werner [1] and Burton-Miller, provide stable formulations for the solution of scattering problems. These are popular approaches, and the development of a multigrid strategy for these would be of interest. Both the methods of implementation and analysis would be different than those in this paper, to account for the different properties of the combined layer operators. Secondly, the methods presented in this paper are not tailored to high-frequency scattering, and our analysis does not include wave-number explicit bounds. Wave-number explicit bounds are described, for example, for combined field operator approaches [8, 9, 10, 22, 20]. The scale resolution condition of kh being sufficiently small (for piecewise linears) needs to be met; in high-frequency settings non-polynomial approximation spaces may be a better approach, [7]. The dependence of the coarsest mesh on the wave number is assumed to satisfy this requirement. In this paper, our focus is on a much simpler situation: how to use a first-kind integral equation with piecewise constant approximants to the solution, in the low to medium frequency situations of scattering from polygonal domains.

We now give a brief derivation of the acoustic single layer equation using the framework of a direct boundary integral approach. We consider the following exterior Helmholtz problem with prescribed Dirichlet data on the boundary of a scatterer. Here, Γ is a simple, closed polygonal curve in the plane and Ω^{ext} denotes its exterior domain.

$$-\Delta u - \kappa^2 u = 0 \quad \text{in } \Omega^{ext}, \quad u = g \quad \text{on } \Gamma \quad \text{and} \quad \lim_{r \rightarrow \infty} r^{\frac{1}{2}} \left(\frac{\partial u}{\partial r} - i\kappa u \right) = 0.$$

To guarantee unique solvability we assume a non-zero, real wave-number $\kappa \in \mathbb{R}$, such that κ^2 is not an interior eigenvalue of $-\Delta$. The Sommerfeld radiation condition is given in terms of the usual radial component r in polar coordinates. It is well known that the solution to this problem is fully determined by its complete Cauchy data $g = \gamma^+ u$ and $\sigma = B_\nu^+ u$, where $\gamma^+ : H_{loc}^1(\Omega^{ext}) \rightarrow H^{1/2}(\Gamma)$ and $B_\nu^+ : H_{loc}^1(\Omega^{ext}) \rightarrow H^{-1/2}(\Gamma)$ denote the exterior trace operator and the exterior conormal derivative respectively. The normal n is assumed to be outward to Ω^{ext} , ie, it points into the bounded region. In fact, for $x \in \Omega^{ext}$ one has an integral representation formula for the solution to the boundary value problem (e.g. [16], [24]), namely

$$u(x) = -\frac{i}{4} \int_{\Gamma} H_0^{(1)}(\kappa|x-y|) \sigma(y) ds_y + \frac{i}{4} \int_{\Gamma} \frac{\partial H_0^{(1)}(\kappa|x-y|)}{\partial n_y} g(y) ds_y. \quad (1)$$

The kernels of the two integrals are given in terms of the Hankel function $H_0^{(1)}(z)$ and its conormal derivative. According to the representation (1), it is sufficient to find the unknown surface density σ . To do this, one exploits the jump relations

of the two integrals, i.e. their behavior in the limit as x approaches Γ from both the interior and the exterior of the scattering domain. These relations appear when we take the trace of equation (1) and lead to the following integral equation for σ :

$$V\sigma = f \in H^{1/2}(\Gamma). \quad (2)$$

Here, the right hand side $f = (\frac{1}{2}I + K)g$ depends on the Dirichlet trace g and requires the evaluation of the double layer operator K . The single layer operator V and the double layer operator K are both defined in terms of singular integrals.

$$\begin{aligned} V : H^{-1/2}(\Gamma) &\rightarrow H^{1/2}(\Gamma), & V\sigma(x) &:= \frac{i}{4} \int_{\Gamma} H_0^{(1)}(\kappa|x-y|) \sigma(y) ds_y & x \in \Gamma, \\ K : H^{1/2}(\Gamma) &\rightarrow H^{1/2}(\Gamma), & K\mu(x) &:= \frac{i}{4} \int_{\Gamma} \frac{\partial H_0^{(1)}(\kappa|x-y|)}{\partial n_y} \mu(y) ds_y & x \in \Gamma. \end{aligned}$$

One should note that the above approach to reformulate the original boundary value problem into an integral equation on Γ is by no means unique. However, several methods lead to a single layer equation of the form (2). In the following, we are interested in the weak form of equation (2). Given $f \in H^{1/2}(\Gamma)$, find $\sigma \in H^{-1/2}(\Gamma)$ such that

$$\mathcal{V}(\sigma, \mu) = \langle f, \mu \rangle \quad \text{for all } \mu \in H^{-1/2}(\Gamma), \quad (3)$$

where the continuous sesquilinear form $\mathcal{V} : H^{-1/2}(\Gamma) \times H^{-1/2}(\Gamma) \rightarrow \mathbb{C}$ is defined by $\mathcal{V}(\sigma, \mu) = \langle V\sigma, \mu \rangle$, and $\langle \cdot, \cdot \rangle$ denotes the duality pairing between $H^{1/2}(\Gamma)$ and $H^{-1/2}(\Gamma)$. The single layer operator which corresponds to the Laplacian will be denoted by Λ .

$$\Lambda : H^{-1/2}(\Gamma) \rightarrow H^{1/2}(\Gamma), \quad \Lambda\sigma(x) := -\frac{1}{2\pi} \int_{\Gamma} \ln(|x-y|) \sigma(y) ds_y \quad x \in \Gamma.$$

We note that the underlying differential operator is the principal part of the Helmholtz operator. Its associated sesquilinear form $\Lambda(\cdot, \cdot)$, defined similarly to $\mathcal{V}(\cdot, \cdot)$ above, is positive definite after the region has been scaled properly (see [24] for details), i.e. there holds

$$\Lambda(\sigma, \sigma) \geq C \|\sigma\|_{H^{-1/2}(\Gamma)}^2 \quad \text{for all } \sigma \in H^{-1/2}(\Gamma). \quad (4)$$

Consequently, it defines an inner product whose induced norm is equivalent to the natural energy norm in $H^{-1/2}(\Gamma)$. This will play an important role in the analysis of Section 3.

The paper is organized as follows: In Section 2 we present a multigrid algorithm for integral equations of the first kind, and introduce a (computable) inner product whose induced norm is equivalent to the natural norm in $H^{-1}(\Gamma)$ on finite dimensional test spaces. The multigrid strategy relies on reformulating

Problem (3) using both the standard inner product in $H^{-1}(\Gamma)$ and the new computable version for piecewise constant functions. We introduce smoothers, and present a matrix version of the algorithm. Section 3 consists of a convergence analysis. The key component is a careful study of the difference between the single layer operators for the Laplacian and for the Helmholtz equation. We conclude this section with a convergence result. Finally, in Section 4 we present some numerical experiments describing the spectral behaviour of the single layer operator, as well as that of the operators used in the reformulated problem. We see, in the context of a smooth curve (a circle) and a Lipschitz curve (a square) how the use of the weaker inner product renders the problem suitable for a multigrid strategy. We conclude by reporting on the convergence behavior of the algorithm applied to simple test cases.

2 A multigrid algorithm

In this section we present the multigrid algorithm, originally proposed in [4] for the positive definite pseudodifferential operators of order minus one, and which was applied to the acoustic case in [13]. The multigrid algorithm is presented below in terms of a smoother, whose definition is postponed to Subsection 2.2. The smoother is realized using a weak base inner product. We make this more precise in Subsection 2.1.

We first establish notations needed to describe the multigrid algorithm. Assume that the polygonal boundary Γ is composed of finitely many straight edges Γ_j . Each Γ_j is meshed by a coarse grid of line segments of length l_j^1 .

We successively refine this grid in a uniform way by breaking each element in half and adding the respective midpoints to the vertices of the next finer level. On every level of refinement $k = 1, 2, \dots, J$, we label the vertices in such a way that $x_1^k, x_2^k, \dots, x_{N_k}^k, x_{N_k+1}^k = x_1^k$ is a counterclockwise enumeration. Now, let ϕ_i^k be the characteristic function of the line segment $\tau_i^k = \text{conv}(x_i^k, x_{i+1}^k)$ ($i = 1, 2, \dots, N_k$) and denote their span by $\mathcal{M}_k := \text{span}\{\phi_i^k\}$. For the sake of easier notation we will suppress the level number k in our notations whenever the context rules out any ambiguity. This construction yields a sequence of nested finite-dimensional spaces

$$\mathcal{M}_1 \subset \mathcal{M}_2 \subset \dots \subset \mathcal{M}_J \subset H^{-1/2}(\Gamma).$$

We now define the discrete operators $V_k : \mathcal{M}_k \rightarrow \mathcal{M}_k$ with the help of the $H^{-1}(\Gamma)$ inner product, denoted by $(\cdot, \cdot)_{-1}$. The defining relation is

$$(V_k \sigma, \mu)_{-1} = \mathcal{V}(\sigma, \mu) \quad \text{for all } \sigma, \mu \in \mathcal{M}_k. \quad (5)$$

Analogously, we choose $f_k \in \mathcal{M}_k$ to satisfy $(f_k, \mu)_{-1} = \langle f, \mu \rangle$ for all $\mu \in \mathcal{M}_k$. Then, on every level k , the equation of interest can be written in operator form as

$$V_k \sigma_k = f_k. \quad (6)$$

In order to describe the algorithm in a function space setting, we shall also need the H^{-1} -projections $Q_k : H^{-1}(\Gamma) \rightarrow \mathcal{M}_k$, which are defined by

$$(Q_k \sigma, \mu)_{-1} = (\sigma, \mu)_{-1} \quad \text{for all } \mu \in \mathcal{M}_k.$$

We further need a family of smoothing operators $R_k : \mathcal{M}_k \rightarrow \mathcal{M}_k$. It is defined precisely in Subsection 2.2, but for now, we just assume that R_k are some given linear operators. Then, given an initial guess $\sigma_0 \in \mathcal{M}_J$, the multigrid iteration computes a sequence of approximate solutions to (6) using an iteration of the form $\sigma_{i+1} = Mg_J(\sigma_i, f_J)$, where $Mg_J(\cdot, \cdot)$ is a mapping of $\mathcal{M}_J \times \mathcal{M}_J$ into \mathcal{M}_J , defined recursively by the following algorithm:

Algorithm 1. Set $Mg_1(\sigma, f) = V_1^{-1}f$. If $k > 1$ we define $Mg_k(\sigma, f)$ recursively as follows:

$$\sigma_1 = \sigma + R_k(f - V_k \sigma), \quad (7)$$

$$Mg_k(\sigma, f) = \sigma_1 + Mg_{k-1}(0, Q_{k-1}(f - V_k \sigma_1)). \quad (8)$$

This is a simple variant of a V-cycle multigrid scheme, which only uses pre-smoothing. Equivalently, we can write the iterative scheme as a linear iteration method

$$\sigma_{i+1} = \sigma_i + B_J(f_J - V_J \sigma_i),$$

with an ‘‘approximate inverse’’ $B_J : \mathcal{M}_J \mapsto \mathcal{M}_J$ defined by

$$B_k f_k = Mg_k(0, f_k) \quad \text{for all } f_k \in \mathcal{M}_k \text{ and } k = 2, \dots, J.$$

This operator is useful as a preconditioner in preconditioned iterative methods. The matrix version of Algorithm 1 is given in Subsection 2.3.

2.1 Discrete inner products

The use of the $H^{-1}(\Gamma)$ inner product in defining the operators V_k and Q_k for the multigrid algorithm confronts us with the question of computability. We will have to work around this issue by introducing equivalent computable inner products. These inner products will be used to define smoothers in Section 2.2.

The problem of calculating the $H^{-1}(\Gamma)$ inner product of two elements in \mathcal{M}_k is related to the solution operator of a second order boundary value problem on the boundary curve, namely

$$-u'' + u = v. \quad (9)$$

Here, $v \in H^{-1}(\Gamma)$ is a given function, u has periodic boundary conditions, and the primes denote differentiation with respect to arc-length. The weak form of this problem is uniquely solvable and we denote the bounded solution operator by $T : H^{-1}(\Gamma) \rightarrow H^1(\Gamma)$. Then, for $v, w \in H^{-1}(\Gamma)$ it is easily verified that $(v, w)_{-1} = (Tv, w)_\Gamma = (v, Tw)_\Gamma$, where $(\cdot, \cdot)_\Gamma$ denotes the complex $L^2(\Gamma)$ -inner product. Unfortunately, the use of the exact solution operator T is infeasible.

Instead, we discretize (9) using a second-order finite difference method. This finite difference method results in an $N_k \times N_k$ linear system with an tridiagonal-like matrix \mathbf{A}_k . We need to introduce some more notation in order to see the details. Functions in \mathcal{M}_k can be represented through their basis expansions with respect to the ϕ_j^k . This is done via the following map:

$$\mathbf{e}_k : \mathcal{M}_k \longrightarrow \mathbb{C}^{N_k}, \quad [\mathbf{e}_k(\sigma)]_i = \frac{1}{l_i^k} (\sigma, \phi_i^k)_\Gamma, \quad (10)$$

where $l_i^k := \text{meas}(\tau_i^k)$. Since the basis functions ϕ_i^k are the (orthogonal) indicator functions of the segments τ_i^k , the basis expansion for any $\sigma \in \mathcal{M}_k$ is $\sigma = \sum_{l=1}^{N_k} [\mathbf{e}_k(\sigma)]_l \phi_l^k$, so the map in (10) gives the vector of coefficients.

We then define the (invertible) operator $A_k : \mathcal{M}_k \longrightarrow \mathcal{M}_k$ through

$$A_k \sigma = \sigma - \sum_{i=1}^{N_k} \left(\frac{[\mathbf{e}(\sigma)]_{i+} - [\mathbf{e}(\sigma)]_i}{l_i^2} - \frac{[\mathbf{e}(\sigma)]_i - [\mathbf{e}(\sigma)]_{i-}}{l_i l_{i-}} \right) \phi_i^k, \quad (11)$$

where we use the notation $i+ = (i+1 \bmod N_k)$ and $i- = (i-1 \bmod N_k)$. As in (11), we will often drop the superscript k and identify l_i^k and l_i to be the same for convenience.

The inverse operator A_k^{-1} or equivalently the inverse matrix \mathbf{A}_k^{-1} serve as approximations for the solution operator T . This motivates the definition of the computable, discrete inner products on the spaces \mathcal{M}_k via

$$[\phi, \psi]_k := (A_k^{-1} \phi, \psi)_\Gamma \quad \text{for all } \phi, \psi \in \mathcal{M}_k. \quad (12)$$

The following lemma shows that $\|\cdot\|_{-1}$ and $[\cdot, \cdot]_k$ are equivalent norms, with the equivalence constants independent of the refinement levels $k = 1, \dots, J$. This result can be found in [4] and [12] for the case of the screen problem when Γ is in fact an open boundary patch or an open line segment respectively. Here, we give a proof for a closed boundary curve Γ . For the analysis we will assume that all the mesh element lengths l_i^k are such that $C_1 h_k \leq l_i^k \leq C_2 h_k$ for some fixed positive constants C_1, C_2 . Here h_k is a representative mesh size, e.g., $h_k = \max(\text{meas}(\tau_i^k))$.

For the proof we need a standard approximation result. Let $\theta \in H^1(\Gamma)$ and let $\theta_k \in \mathcal{M}_k$ denote the piecewise constant approximation defined by

$$\theta_k := \sum_{i=1}^{N_k} \theta(x_i^k) \phi_i^k. \quad (13)$$

This is well defined for θ in $H^1(\Gamma)$ by the Sobolev inequality

$$\|\theta\|_{L^\infty(\Gamma)} \leq C \|\theta\|_{H^1(\Gamma)} \quad \text{for all } \theta \in H^1(\Gamma). \quad (14)$$

Then

$$\|\theta - \theta_k\|_{L^2(\Gamma)} \leq C h_k \|\theta\|_{H^1(\Gamma)} \quad \text{for all } \theta \in H^1(\Gamma). \quad (15)$$

To prove this, it suffices to observe that

$$\begin{aligned}
\|\theta - \theta_k\|_{L^2(\tau_i^k)}^2 &= \int_{\tau_i^k} |\theta(x) - \theta(x_i^k)|^2 dx = \int_{\tau_i^k} \left| \int_{x_i^k}^x \theta'(\xi) d\xi \right|^2 dx \\
&\leq \int_{\tau_i^k} \left(\int_{x_i^k}^{x_{i+1}^k} |\theta'(\xi)|^2 d\xi \right) (x - x_i^k) dx \\
&= \frac{l_i^2}{2} \left(\int_{\tau_i^k} |\theta'(\xi)|^2 d\xi \right) = \frac{l_i^2}{2} |\theta|_{H^1(\tau_i^k)}^2.
\end{aligned}$$

Equation (15) follows by summing over all elements. We will use (15) in the proof of the next lemma.

Lemma 1. *There exist constants $c, C > 0$ independent of J such that*

$$c\|\sigma\|_{-1}^2 \leq [\sigma, \sigma]_k \leq C\|\sigma\|_{-1}^2 \quad \text{for } \sigma \in \mathcal{M}_k \quad (k = 1, \dots, J). \quad (16)$$

Proof. Given an element

$$\sigma = \sum_{i=1}^{N_k} [\mathbf{e}(\sigma)]_i \phi_i^k, \quad \text{we define} \quad \tilde{\sigma} = \sum_{i=1}^{N_k} [\mathbf{e}(\sigma)]_i \psi_i^k,$$

where ψ_i^k is the continuous and piecewise linear function which takes the value one at node x_i^k and vanishes at every other node (otherwise known as the ‘‘hat’’ function). Note that $\tilde{\sigma}$ is in $H^1(\Gamma)$. Then applying (15) to $\tilde{\sigma}$, we obtain

$$\|\sigma - \tilde{\sigma}\|_{L^2(\Gamma)} \leq C h_k \|\partial \tilde{\sigma}\|_{L^2(\Gamma)},$$

where $\partial \tilde{\sigma}$ denotes the derivative of $\tilde{\sigma}$ with respect to arc length. Note that

$$\partial \tilde{\sigma} = \sum_i \left(\frac{[\mathbf{e}(\sigma)]_{i+} - [\mathbf{e}(\sigma)]_i}{l_i} \right) \phi_i^k. \quad (17)$$

From this it follows by straight forward calculations that

$$|\tilde{\sigma}|_{H^1(\Gamma)}^2 \leq C h_k^{-2} \|\sigma\|_{L^2(\Gamma)}^2. \quad (18)$$

Before proving the inequalities, we make a few observations. Using the operator from (11) we see for $\sigma, \mu \in \mathcal{M}_k$,

$$\begin{aligned}
&(A_k \sigma, \mu)_\Gamma \\
&= (\sigma, \mu)_\Gamma - \sum_i \int_{\tau_i} \left(\frac{[\mathbf{e}(\sigma)]_{i+} - [\mathbf{e}(\sigma)]_i}{l_i^2} \phi_i - \frac{[\mathbf{e}(\sigma)]_i - [\mathbf{e}(\sigma)]_{i-}}{l_i l_{i-}} \phi_i \right) \overline{[\mathbf{e}(\mu)]_i} \phi_i ds \\
&= (\sigma, \mu)_\Gamma - \sum_i \left(\frac{[\mathbf{e}(\sigma)]_{i+} - [\mathbf{e}(\sigma)]_i}{l_i} - \frac{[\mathbf{e}(\sigma)]_i - [\mathbf{e}(\sigma)]_{i-}}{l_{i-}} \right) \overline{[\mathbf{e}(\mu)]_i} \\
&= (\sigma, \mu)_\Gamma + \sum_i ([\mathbf{e}(\sigma)]_{i+} - [\mathbf{e}(\sigma)]_i) \left(\overline{[\mathbf{e}(\mu)]_{i+}} - \overline{[\mathbf{e}(\mu)]_i} \right) \frac{1}{l_i} \\
&= (\sigma, \mu)_\Gamma + \int_\Gamma \partial \tilde{\sigma} \overline{\partial \tilde{\mu}} ds.
\end{aligned}$$

by (17). The right hand side above defines a sesquilinear form

$$a(\tilde{\sigma}, \tilde{\mu}) = (\sigma, \mu)_\Gamma + (\partial\tilde{\sigma}, \partial\tilde{\mu})_\Gamma.$$

It is easy to see that $\|\sigma\|_{L^2(\Gamma)}^2 \sim \|\tilde{\sigma}\|_{L^2(\Gamma)}^2$, where $X \sim Y$ indicates that $C_1X \leq Y \leq C_2Y$ holds with some positive constants C_1 and C_2 independent of the mesh. Thus we have proven that

$$\|\tilde{\sigma}\|_{H^1(\Gamma)}^2 \sim a(\tilde{\sigma}, \tilde{\sigma}) \equiv (A_k\sigma, \sigma), \quad \text{for all } \sigma \in \mathcal{M}_k.$$

If we combine the above norm equivalence with (18) and write $\|\sigma\|_{A_k}^2 = (A_k\sigma, \sigma)$, it immediately follows that

$$\|\sigma\|_{A_k}^2 = a(\tilde{\sigma}, \tilde{\sigma}) = \|\sigma\|_{L^2(\Gamma)}^2 + |\tilde{\sigma}|_{H^1(\Gamma)}^2 \leq (1 + C h_k^{-2}) \|\sigma\|_{L^2(\Gamma)}^2 \leq C h_k^{-2} \|\sigma\|_{L^2(\Gamma)}^2.$$

Here, C denotes a generic constant independent of meshsize. In other words, this yields the inequality

$$\lambda_{\max}(A_k) \leq C h_k^{-2}, \quad (19)$$

which could also be shown using other methods.

We now begin proving the inequalities of the lemma, starting with the second inequality in (16).

$$\begin{aligned} (A_k\sigma, \sigma)_\Gamma &= a(\tilde{\sigma}, \tilde{\sigma}) = \sup_{\mu \in \mathcal{M}_k} \frac{|a(\tilde{\sigma}, \tilde{\mu})|^2}{a(\tilde{\mu}, \tilde{\mu})} \leq C \sup_{\mu \in \mathcal{M}_k} \frac{|(A_k\sigma, \mu)_\Gamma|^2}{C_1 \|\tilde{\mu}\|_{H^1(\Gamma)}^2} \\ &\leq C \sup_{\mu \in \mathcal{M}_k} \frac{|(A_k\sigma, \tilde{\mu})_\Gamma|^2 + |(A_k\sigma, \mu - \tilde{\mu})_\Gamma|^2}{\|\tilde{\mu}\|_{H^1(\Gamma)}^2} \\ &\leq C \sup_{\mu \in \mathcal{M}_k} \frac{|(A_k\sigma, \tilde{\mu})_\Gamma|^2}{\|\tilde{\mu}\|_{H^1(\Gamma)}^2} + \frac{\|A_k\sigma\|_{L^2(\Gamma)}^2 \|\mu - \tilde{\mu}\|_{L^2(\Gamma)}^2}{\|\tilde{\mu}\|_{H^1(\Gamma)}^2} \\ &\leq C \sup_{\mu \in H^1(\Gamma)} \frac{|(A_k\sigma, \mu)_\Gamma|^2}{\|\mu\|_{H^1(\Gamma)}^2} + C h_k^2 \|A_k\sigma\|_{L^2(\Gamma)}^2 \\ &= C \left(\|A_k\sigma\|_{H^{-1}(\Gamma)}^2 + h_k^2 \|A_k\sigma\|_{L^2(\Gamma)}^2 \right). \end{aligned} \quad (20)$$

The inverse inequality

$$\|\mu\|_{L^2(\Gamma)} \leq C h_k^{-1} \|\mu\|_{H^{-1}(\Gamma)} \quad \text{for all } \mu \in \mathcal{M}_k \quad (21)$$

can be found in [4, Eq. (3.20)]. Using it in (20), we get the upper bound

$$(A_k\sigma, \sigma)_\Gamma \leq C \|A_k\sigma\|_{H^{-1}(\Gamma)}^2 \quad \text{for all } \sigma \in \mathcal{M}_k \quad (22)$$

or equivalently

$$(A_k^{-1}\mu, \mu)_\Gamma \leq C \|\mu\|_{H^{-1}(\Gamma)}^2 \quad \text{for all } \mu \in \mathcal{M}_k. \quad (23)$$

This is the upper inequality stated in the lemma.

It remains to prove the first inequality in (16). For this, we need a stability result for the L^2 -orthogonal projection $\Pi_k : H^1(\Gamma) \rightarrow \mathcal{M}_k$, namely

$$(A_k \Pi_k \theta, \Pi_k \theta) \leq C \|\theta\|_{H^1(\Gamma)}^2. \quad (24)$$

The result (24) follows once we prove that for all $\theta \in H^1(\Gamma)$, there exists $\theta_k \in \mathcal{M}_k$, such that

$$\|\theta_k\|_{A_k} \leq C \|\theta\|_{H^1(\Gamma)} \quad (25)$$

$$\|\theta - \theta_k\|_{L^2(\Gamma)} \leq C h_k |\theta|_{H^1(\Gamma)}. \quad (26)$$

Indeed, writing $\Pi_k \theta = \Pi_k(\theta - \theta_k) + \theta_k$,

$$\begin{aligned} \|\Pi_k \theta\|_{A_k} &\leq \|\Pi_k(\theta - \theta_k)\|_{A_k} + \|\theta_k\|_{A_k} \\ &\leq C h_k^{-1} \|\Pi_k(\theta - \theta_k)\|_{L^2(\Gamma)} + \|\theta_k\|_{A_k} && \text{by (19)} \\ &\leq C h_k^{-1} \|(\theta - \theta_k)\|_{L^2(\Gamma)} + C \|\theta\|_{H^1(\Gamma)} && \text{by (25)} \\ &\leq C \|\theta\|_{H^1(\Gamma)} && \text{by (26)}. \end{aligned}$$

Therefore, let us now exhibit a θ_k satisfying (25) and (26).

Consider the θ_k defined in (13). By (15), we get (26). That θ_k also satisfies (25) is seen using the L^2 -orthogonal projection \mathcal{Q}_k into the space of continuous functions on Γ that are linear on each τ_i^k . It is well known that \mathcal{Q}_k is stable in the $H^1(\Gamma)$ -norm [6]. Hence, using the standard approximation properties of the projection $\mathcal{Q}_k \theta$ and the linear interpolant $\tilde{\theta}_k$ of θ , we find

$$\begin{aligned} |\tilde{\theta}_k|_{H^1(\Gamma)} &\leq |\tilde{\theta}_k - \mathcal{Q}_k \theta|_{H^1(\Gamma)} + |\mathcal{Q}_k \theta|_{H^1(\Gamma)} \\ &\leq C h_k^{-1} \|\tilde{\theta}_k - \mathcal{Q}_k \theta\|_{L^2(\Gamma)} + |\mathcal{Q}_k \theta|_{H^1(\Gamma)} \\ &\leq C h_k^{-1} (\|\tilde{\theta}_k - \theta\|_{L^2(\Gamma)} + \|\theta - \mathcal{Q}_k \theta\|_{L^2(\Gamma)}) + |\mathcal{Q}_k \theta|_{H^1(\Gamma)} \\ &\leq C \|\theta\|_{H^1(\Gamma)}. \end{aligned} \quad (27)$$

Moreover, by the Sobolev inequality (14), we also have

$$\|\theta_k\|^2 = \sum_i |\theta(x_i)|^2 \|\phi_i\|^2 \leq \|\theta\|_{H^1(\Gamma)}^2 \left(\sum_i \int_{\tau_i} 1 \right) \leq C \|\theta\|_{H^1(\Gamma)}^2. \quad (28)$$

Therefore, combining (27) and (28), we have

$$\|\theta_k\|_{A_k}^2 = \|\theta_k\|_{L^2(\Gamma)}^2 + |\tilde{\theta}_k|_{H^1(\Gamma)}^2 \leq C \|\theta\|_{H^1(\Gamma)}^2,$$

which proves (25).

To complete the proof of the first inequality in (16) of the lemma,

$$\begin{aligned} \|\sigma\|_{H^{-1}(\Gamma)}^2 &= \sup_{\theta \in H^1(\Gamma)} \frac{(\sigma, \theta)^2}{\|\theta\|_{H^1(\Gamma)}^2} = \sup_{\theta \in H^1(\Gamma)} \frac{(\sigma, \Pi_k \theta)^2}{\|\theta\|_{H^1(\Gamma)}^2} \\ &\leq C \sup_{\theta \in H^1(\Gamma)} \frac{(\sigma, \Pi_k \theta)^2}{(A_k \Pi_k \theta, \Pi_k \theta)} = C (A_k^{-1} \sigma, \sigma), \end{aligned}$$

where we have used (24).

2.2 Smoothers

Using the inner products from Section 2.1 we can define a simple Richardson smoother suitable for multigrid algorithms (see for example [2]). The smoother is given by

$$[R_k \sigma, \theta]_k = \frac{1}{\tilde{\lambda}_k} (\sigma, \theta)_{-1}, \quad (29)$$

where $\tilde{\lambda}_k$ is related to the Rayleigh-Ritz quotient involving the *positive definite* sesquilinear form $\Lambda(\cdot, \cdot)$, namely

$$\lambda_k = \sup_{\theta \in \mathcal{M}_k} \frac{\Lambda(\theta, \theta)}{[\theta, \theta]_k}, \quad (30)$$

as follows: We assume for our analysis that $\tilde{\lambda}_k$ is a number that satisfies

$$\lambda_k \leq \tilde{\lambda}_k \leq C \lambda_k \quad (31)$$

for some mesh independent constant C .

Define the operator Λ_k as in (5) but with the sesquilinear form $\mathcal{V}(\cdot, \cdot)$ replaced by $\Lambda(\cdot, \cdot)$. The eigenvalue λ_k is then a computable version of the largest eigenvalue of the operator Λ_k with respect to the minus one inner product. In practice, we could choose $\tilde{\lambda}_k = \lambda_k$, or an approximation to λ_k computed by a few iterations of the power method.

2.3 Matrix version

Now we give a readily implementable matrix version of the previously given multigrid algorithm. Since $\mathcal{M}_k \subseteq \mathcal{M}_{k+1}$ we can find numbers $c_{i,l}$ such that $\phi_i^k = \sum_{l=1}^{N_{k+1}} c_{i,l} \phi_l^{k+1}$. These entries define the $N_k \times N_{k+1}$ restriction matrix \mathbf{C}_k by $[\mathbf{C}_k]_{i,l} = c_{i,l}$. This matrix and its transpose are used as intergrid transfer operators. We further define the operator

$$\mathbf{f}_k : \mathcal{M}_k \longrightarrow \mathbb{C}^{N_k}, \quad [\mathbf{f}_k(\sigma)]_i = (\sigma, \phi_i^k)_{-1}. \quad (32)$$

Algorithm 1 can then be translated into an approximation scheme for the matrix version $\mathbf{V}_J \mathbf{u} = \mathbf{b}$ of equation (6). Here, the vectors are given by $\mathbf{b} = \mathbf{f}_k(f_J)$ and $\mathbf{u} = \mathbf{e}_k(\sigma_J)$ and the system matrix is $\mathbf{V}_J = [\langle V_J \phi_j^J, \phi_i^J \rangle]_{i,j}$. This yields a procedure $\mathbf{Mg}_J(\mathbf{s}, \mathbf{b})$ that outputs an approximation to the solution given an input iterate \mathbf{s} . To describe it we will also need a matrix of the operator A_k , which we denote by \mathbf{A}_k . Specifically \mathbf{A}_k is the matrix satisfying $\mathbf{e}_k(A_k \sigma) = \mathbf{A}_k \mathbf{e}_k(\sigma)$. It is a circulant matrix with cyclically shifted rows of the form

$$\mathbf{A}_k = \text{Circulant} [0 \cdots 0, \quad -(l_i l_{i-})^{-1}, \quad 1 + l_i^{-2} + (l_i l_{i-})^{-1}, \quad -l_i^{-2}, \quad 0 \cdots 0].$$

Note that \mathbf{A}_k is neither tridiagonal nor symmetric, but $\mathbf{H}_k \mathbf{A}_k$ is symmetric, where \mathbf{H}_k is a diagonal matrix whose i^{th} diagonal entry is $\text{meas}(\tau_i^k)$. The translation of Algorithm 1 into its matrix version is done via the identities of the following lemma.

Lemma 2. *The following identities hold:*

$$\mathbf{f}_k(V_k g) = \mathbf{V}_k \mathbf{e}_k(g), \quad \text{for all } g \in \mathcal{M}_k, \quad (33)$$

$$\mathbf{f}_{k-1}(Q_{k-1} g) = \mathbf{C}_{k-1} \mathbf{f}_k(g) \quad \text{for all } g \in \mathcal{M}_k, \quad (34)$$

$$\mathbf{e}_k(g) = \mathbf{C}_{k-1}^t \mathbf{e}_{k-1}(g) \quad \text{for all } g \in \mathcal{M}_{k-1}, \quad (35)$$

$$\mathbf{e}_k(R_k g) = \tilde{\lambda}_k^{-1} \mathbf{H}_k^{-1} \mathbf{A}_k^t \mathbf{f}_k(g) \quad \text{for all } g \in \mathcal{M}_k, \quad (36)$$

$$\mathbf{e}_1(V_1^{-1} g) = \mathbf{V}_1^{-1} \mathbf{f}_1(g) \quad \text{for all } g \in \mathcal{M}_1. \quad (37)$$

Proof. Let us prove (33):

$$\begin{aligned} [\mathbf{f}_k(V_k g)]_i &= (V_k g, \phi_i^k)_{-1} = \mathcal{V}(g, \phi_i^k) \\ &= \sum_{j=1}^{N_k} [\mathbf{e}_k(g)]_j \mathcal{V}(\phi_j^k, \phi_i^k) = \sum_{j=1}^{N_k} [\mathbf{V}_k]_{i,j} [\mathbf{e}_k(g)]_j \\ &= [\mathbf{V}_k \mathbf{e}_k(g)]_i. \end{aligned}$$

Next, let us prove (34):

$$\begin{aligned} [\mathbf{f}_{k-1}(Q_{k-1} g)]_i &= (Q_{k-1} g, \phi_i^{k-1})_{-1} = (g, \phi_i^{k-1})_{-1} = (g, \sum_{l=1}^{N_k} [\mathbf{C}_{k-1}]_{i,l} \phi_l^k)_{-1} \\ &= [\mathbf{C}_{k-1} \mathbf{f}_k(g)]_i, \end{aligned}$$

since \mathbf{C}_{k-1} is real. The proof of (35) is similar. To prove (36), observe that

$$\frac{1}{\tilde{\lambda}_k} [\mathbf{f}_k(g)]_i \equiv \frac{1}{\tilde{\lambda}_k} (g, \phi_i^k)_{-1} = [R_k g, \phi_i^k]_k = [\mathbf{H}_k \mathbf{A}_k^{-1} \mathbf{e}_k(R_k g)]_i.$$

Multiplying both sides by the symmetric matrix $\mathbf{A}_k \mathbf{H}_k^{-1}$, we obtain (36). Proofs of the other identities are similar.

These identities enable us to state a matrix version of Algorithm 1. For example, applying \mathbf{e}_k to the step (7) of Algorithm 1 and using (36) and using Lemma 2, we have

$$\begin{aligned} \mathbf{e}_k(\sigma_1) &= \mathbf{e}_k(\sigma) + \mathbf{e}_k(R_k(f - V_k \sigma)) = \mathbf{e}_k(\sigma) + \tilde{\lambda}_k^{-1} \mathbf{H}_k^{-1} \mathbf{A}_k^t \mathbf{f}_k(f - V_k \sigma) \\ &= \mathbf{e}_k(\sigma) + \tilde{\lambda}_k^{-1} \mathbf{H}_k^{-1} \mathbf{A}_k^t (\mathbf{f}_k(f) - \mathbf{V}_k \mathbf{e}_k(\sigma)). \end{aligned}$$

Thus, the matrix version of this step is $\mathbf{s}_1 = \mathbf{s} + \tilde{\lambda}_k^{-1} \mathbf{H}_k^{-1} \mathbf{A}_k^t (\mathbf{b} - \mathbf{V}_k \mathbf{s})$ with $\mathbf{s}_1 = \mathbf{e}_k(\sigma_1)$, $\mathbf{s} = \mathbf{e}_k(\sigma)$, and $\mathbf{b} = \mathbf{f}_k(f)$. Using also the other identities in (33)–(37), we can similarly translate the entire algorithm. We then obtain the following matrix version of the algorithm $\mathbf{Mg}_J(\mathbf{s}, \mathbf{b})$, which outputs an approximation for the solution of the matrix equation $\mathbf{V}_J \mathbf{u} = \mathbf{b}$, given an input iterate \mathbf{s} .

Algorithm 2. *Let \mathbf{s} and \mathbf{b} be any given vectors in \mathbb{C}^{N_k} . Define $\mathbf{Mg}_k(\mathbf{s}, \mathbf{b})$ recursively as follows. Set $\mathbf{Mg}_1(\mathbf{s}, \mathbf{b}) = \mathbf{V}_1^{-1} \mathbf{b}$. If $k > 1$, define $\mathbf{Mg}_k(\mathbf{s}, \mathbf{b})$ as the vector in \mathbb{C}^{N_k} obtained recursively by:*

$$\begin{aligned} \mathbf{s}_1 &= \mathbf{s} + \tilde{\lambda}_k^{-1} \mathbf{H}_k^{-1} \mathbf{A}_k^t (\mathbf{b} - \mathbf{V}_k \mathbf{s}), \\ \mathbf{Mg}_k(\mathbf{s}, \mathbf{b}) &= \mathbf{s}_1 + \mathbf{C}_{k-1}^t \mathbf{Mg}_{k-1}(0, \mathbf{C}_{k-1} (\mathbf{b} - \mathbf{V}_k \mathbf{s}_1)). \end{aligned}$$

It is important to note that the inverse of \mathbf{A}_k is not needed in the implementation. We only need to multiply by \mathbf{A}_k^t . In the case of a uniform mesh with mesh size h_k the multiplication by the matrix \mathbf{H}_k^{-1} reduces to multiplication with the constant $1/h_k$. Furthermore, it has been shown in [4] that

$$\lambda_k = O(1/h_k). \quad (38)$$

Motivated by this observation, we could replace the expression $\tilde{\lambda}_k^{-1} \mathbf{H}_k^{-1}$ in Algorithm 2 by C , for some constant C (which depends on the geometry of the domain). This would allow us to bypass the eigenvalue computation, which would otherwise be inherent in the algorithm. The numerical experiments we present later, however, explicitly include the expression $\tilde{\lambda}_k^{-1} \mathbf{H}_k^{-1}$.

Note that a matrix preconditioner \mathbf{B}_k for \mathbf{V}_k is implicit in Algorithm 2 and is defined by $\mathbf{B}_k \mathbf{b} = \mathbf{Mg}_k(0, \mathbf{b})$. A theoretical study of the convergence rate of the algorithm is presented in the next section.

3 Convergence Analysis

3.1 Preliminary Steps

Before we can give a detailed description of the convergence behavior of Algorithm 1, we need to pave the way with some preliminary discussions. In particular, we need the Galerkin projections $P_k : H^{-1/2}(\Gamma) \rightarrow \mathcal{M}_k$ satisfying

$$\mathcal{V}(P_k \sigma, \mu) = \mathcal{V}(\sigma, \mu) \quad \text{for all } \mu \in \mathcal{M}_k. \quad (39)$$

As we see next, such operators are well defined once the mesh size is sufficiently small. The assumption on the wave number that κ^2 is not an interior eigenvalue of $-\Delta$ implies that for homogeneous right hand side the equation $V\sigma = 0$ only has the trivial solution $\sigma = 0$. It is then a standard theorem on compact perturbations (see for example [23, Theorem 4.2.9]), that the discretized version of equation (2) has a unique solution $\sigma_k \in \mathcal{M}_k$ if the corresponding meshsize h_k is sufficiently small. Furthermore, we know that the Galerkin solutions σ_k converge quasi-optimally to the true solution σ , i.e.

$$\|\sigma - \sigma_k\|_{H^{-1/2}(\Gamma)} \leq C \min_{v_k \in \mathcal{M}_k} \|\sigma - v_k\|_{H^{-1/2}(\Gamma)}.$$

Also, once the mesh size is sufficiently small, the Galerkin solutions depend continuously on the data, i.e.,

$$\|\sigma_k\|_{H^{-1/2}(\Gamma)} \leq C \|f\|_{H^{1/2}(\Gamma)}. \quad (40)$$

As a consequence, we immediately have the following lemma which shows that P_1 is a well defined continuous operator once h_1 is small enough (and so is P_k for $k > 1$). In the lemma and elsewhere, we write $\|\cdot\|_\Lambda$ for the vector norm $\Lambda(\cdot, \cdot)^{1/2}$. We will also use the same notation for the operator norm induced by this vector norm.

Lemma 3. *There exists an $H > 0$ such that once the coarse mesh size h_1 is less than H , there is a unique $P_k\sigma$ satisfying (39) for all $k \geq 1$ and moreover,*

$$\|P_k\sigma\|_\Lambda \leq C \|\sigma\|_\Lambda. \quad (41)$$

Now let us introduce a few ingredients needed to analyze the multigrid algorithm. A simple induction argument shows that $Mg_k(\cdot, \cdot)$ as defined in Algorithm 1 is linear as a mapping from $\mathcal{M}_k \times \mathcal{M}_k$ into \mathcal{M}_k . It is also consistent in the sense that $\sigma_k = Mg_k(\sigma_k, V_k\sigma_k)$ holds for all $\sigma_k \in \mathcal{M}_k$. The error reduction operator of the scheme is given by

$$\mathbf{E} = Mg_J(\cdot, 0), \quad (42)$$

i.e., if e^i denotes the error at step i , we have $e^{i+1} = Mg_J(e^i, 0)$. Furthermore, the error reduction operator admits a product representation as shown in Lemma 4. This representation will be essential in the convergence analysis of the V-cycle scheme. Proofs of such results can be found in [2].

Lemma 4. *Let $T_k = R_k V_k P_k$ for $k \geq 2$ and set $T_1 = P_1$. For $k \geq 1$ we then define $E_k u = u - Mg_k(0, V_k P_k u)$ and set $E_0 = I$, the identity operator. Then,*

$$E_k = E_{k-1}(I - T_k), \quad \text{and} \quad (43)$$

$$\mathbf{E} = (I - T_1)(I - T_2) \cdots (I - T_J). \quad (44)$$

The same representation holds for the error reduction operator $\tilde{\mathbf{E}}$ of the definite problem. Analogous to (39), we can define \tilde{P}_k as the orthogonal projection into \mathcal{M}_k with respect to the $\Lambda(\cdot, \cdot)$ -inner product. This is the Galerkin projection for the principal part of the differential operator. If we set $\tilde{T}_k = R_k \Lambda_k \tilde{P}_k$, we get

$$\tilde{\mathbf{E}} = (I - \tilde{T}_1) \cdots (I - \tilde{T}_J). \quad (45)$$

This operator is proved to be a reducer in [4]. Specifically, in [4] the convergence for the symmetric version of the multigrid algorithm applied to the positive definite problem was shown. In fact, it was shown that the symmetric error reduction operator \tilde{E}^s in this case is bounded away from 1 independently of the number of levels of refinement. The symmetric version differs from Algorithm 1 by an additional post-smoothing step. However, it is well known (see, e.g., [5, Remark 3.4]) that the analogous result holds for Algorithm 1 with just the pre-smoothing, i.e., we have the following theorem.

Theorem 1. *The error reduction operator $\tilde{\mathbf{E}}$ for Algorithm 1 applied to the positive definite problem satisfies*

$$\|\tilde{\mathbf{E}}\|_\Lambda \leq \tilde{\delta} < 1, \quad (46)$$

where $\tilde{\delta}$ is independent of J .

In order to analyze the algorithm for the indefinite Helmholtz case we look at the difference between \mathbf{E} and $\tilde{\mathbf{E}}$. Let $Z_k = T_k - \tilde{T}_k$, and suppose for some positive α we have

$$\|Z_k\|_\Lambda \leq C_1 h_k^\alpha \quad \text{for } k = 1, \dots, J. \quad (47)$$

With this assumption, by well known arguments in an abstract multigrid setting [2, 14], we have the following theorem.

Theorem 2. *Let \mathbf{E} satisfy (44) and $\tilde{\mathbf{E}}$ satisfy (45). Assume that (47) holds. Then, there exists a positive constant C_2 depending on C_1 , h_1 , and α above, such that:*

$$\|\mathbf{E}\|_\Lambda \leq \|\tilde{\mathbf{E}}\|_\Lambda + C_2 h_1^\alpha. \quad (48)$$

We know that $\|\tilde{\mathbf{E}}\|_\Lambda \leq \tilde{\delta} < 1$ by Theorem 1. Hence by virtue of Theorem 2, to prove a convergence result for our multigrid application, we only need to verify the hypotheses of Theorem 2, namely (47). This will be done in Subsection 3.2.

Before concluding this subsection, we need to establish one more ingredient for the multigrid perturbation argument. It is well known that the difference between the single layer potentials of the Helmholtz and the Laplace equations, namely $D := V - \Lambda$, is compact as a map $H^{-1/2}(\Gamma) \rightarrow H^{1/2}(\Gamma)$. For our purposes we need the following lemma.

Lemma 5. *D is bounded as a map $H^{-1/2}(\Gamma) \rightarrow H^1(\Gamma)$.*

Proof. In this proof, we use the explicit integral representation of the single layer potentials as given in Section 1. The operator $D = V - \Lambda$ generates the sesquilinear form

$$D(\mu, \sigma) = \langle D\mu, \sigma \rangle,$$

and is an integral operator whose kernel consists of the function

$$f(x, y) = g(|x - y|) \quad \text{where} \quad g(z) = \frac{i}{4} H_0^{(1)}(\kappa z) + \frac{1}{2\pi} \ln(z).$$

The function g has the following asymptotic behavior as z approaches 0:

$$g(z) \sim c_1 + O(z^2 \log z) \quad (49)$$

$$g'(z) \sim c_2(z \log z) + O(z) \quad (50)$$

$$g''(z) \sim c_3 + O(\log z), \quad (51)$$

for some constants c_i (depending on κ).

Let us now estimate the H^1 -norm of $D\sigma$. Denote by ∂f the derivative of f with respect to arc length along Γ . Then

$$\|D\sigma\|_{H^1(\Gamma)}^2 = \|D\sigma\|_{L^2(\Gamma)}^2 + \|\partial(D\sigma)\|_{L^2(\Gamma)}^2. \quad (52)$$

Let us start by bounding the first term on the right hand side. Letting $F_x(y) \equiv f(x, y)$, we have

$$\begin{aligned} \|D\sigma\|_{L^2(\Gamma)}^2 &= \int_{\Gamma} \left| \int_{\Gamma} f(x, y)\sigma(y) ds_y \right|^2 ds_x \\ &\leq \int_{\Gamma} \|F_x\|_{H^{1/2}(\Gamma)}^2 \|\sigma\|_{H^{-1/2}(\Gamma)}^2 ds_x. \end{aligned} \quad (53)$$

By the trace theorem

$$\|F_x\|_{H^{1/2}(\Gamma)} \leq C\|F_x\|_{H^1(B_r)},$$

for some ball B_r of sufficiently large radius r (so that B_r contains Γ). The term $\|F_x\|_{H^1(B_r)}$ is finite because

$$\nabla_y F_x = g'(|x-y|) \frac{x-y}{|x-y|}, \quad (54)$$

is a square integrable function (due to (50) and the boundedness of $(x-y)/|x-y|$).

By a change of variable (mapping x to 0), integrals of F_x can be converted to integrals of F_0 on transformed domains. Hence, by enlarging the transformed integration region, we have

$$\|F_x\|_{H^1(B_r)} \leq \|F_0\|_{H^1(B_{2r})}.$$

This shows that the first factor in the integrand of (53) admits a bound independent of the integration variable x , so

$$\begin{aligned} \|D\sigma\|_{L^2(\Gamma)}^2 &\leq \int_{\Gamma} \|F_x\|_{H^{1/2}(\Gamma)}^2 \|\sigma\|_{H^{-1/2}(\Gamma)}^2 ds_x \\ &\leq \text{meas}(\Gamma) C \|F_0\|_{H^1(B_{2r})}^2 \|\sigma\|_{H^{-1/2}(\Gamma)}^2 \\ &\leq C \|\sigma\|_{H^{-1/2}(\Gamma)}^2. \end{aligned} \quad (55)$$

We treat the second term in (52) similarly. Denote by t_x the unit tangential vector to Γ in the point $x \in \Gamma$, which is defined everywhere except on a set of measure zero (the corners). Then,

$$\begin{aligned} \|\partial D\sigma\|_{L^2(\Gamma)}^2 &= \int_{\Gamma} \left| \left(\nabla_x \int_{\Gamma} f(x, y)\sigma(y) ds_y \right) \cdot t_x \right|^2 ds_x \\ &= \int_{\Gamma} \left| \int_{\Gamma} (\nabla_x f(x, y)) \cdot t_x \sigma(y) ds_y \right|^2 ds_x \\ &\leq \int_{\Gamma} \|G_x\|_{H^{1/2}(\Gamma)}^2 \|\sigma\|_{H^{-1/2}(\Gamma)}^2 ds_x \end{aligned} \quad (56)$$

where

$$G_x(y) = t_x \cdot \nabla_x f(x, y) = -t_x \cdot \nabla_y F_x.$$

Note that by differentiating (54),

$$\nabla_y G_x = -g''(|x-y|) \frac{(x-y) \cdot t_x}{|x-y|^2} (x-y) - g'(|x-y|) \nabla_y \left(\frac{(x-y) \cdot t_x}{|x-y|} \right).$$

The term $\nabla_y(x-y) \cdot t_x/|x-y|$ is $O(1/|x-y|)$, while the multiplying factor $g'(|x-y|)$ is $O(|x-y| \log|x-y|)$ by (50). Hence the last term is $O(\log|x-y|)$. The first term on the right hand side is also $O(\log|x-y|)$, because of (51). Consequently, $\nabla_y G_x$ is locally square integrable on \mathbb{R}^2 . Therefore, returning to (56), we can complete the estimation using a trace inequality and bounding $\|G_x\|_{H^{1/2}(\Gamma)}^2$ independently of x as before. Thus

$$\|\partial D\sigma\|_{L^2(\Gamma)}^2 \leq C\|\sigma\|_{H^{-1/2}(\Gamma)}^2. \quad (57)$$

Using (57) and 55 in (52), the proof is finished.

3.2 Convergence

Now we give our main result on the convergence of the multigrid algorithm for our application. The proof proceeds by verifying the hypotheses of Theorem 2. For this, we need a regularity result. Consider the solution ε of the adjoint problem

$$\mathcal{V}(\eta, \varepsilon) = \overline{F(\eta)} \quad \text{for all } \eta \in H^{-1/2}(\Gamma), \quad (58)$$

for some linear functional F on $H^{-1/2}(\Gamma)$, or in other words F is in $H^{1/2}(\Gamma)$. If F is more regular, then we expect the solution ε to be more regular.

To make this precise, note that (58) can be rewritten as

$$\overline{\mathcal{V}(\varepsilon, \eta)} = F(\eta),$$

where $\overline{\mathcal{V}(\cdot, \cdot)}$ is defined for smooth σ, μ by

$$\overline{\mathcal{V}(\sigma, \mu)} = \int_{\Gamma} \int_{\Gamma} \overline{\frac{i}{4} H_0^{(1)}(\kappa|x-y|) \sigma(y) \overline{\mu(x)}} ds_y ds_x.$$

This form extends continuously to $H^{-1/2}(\Gamma) \times H^{-1/2}(\Gamma)$ and the operator $V^* : H^{-1/2}(\Gamma) \mapsto H^{1/2}(\Gamma)$ defined by $\langle V^* \sigma, \mu \rangle = \overline{\mathcal{V}(\sigma, \mu)}$ is continuous. It can be written as

$$V^* = \Lambda + D^*$$

where D^* is an integral operator analogously to D , but with an integral kernel conjugate to that of D . The same type of arguments as in Lemma 5 show that

$$D^* : H^{-1/2}(\Gamma) \mapsto H^1(\Gamma)$$

is continuous. Now, it is well known [23, Thm. 3.2.2] that for the positive definite problem $\Lambda u = F$, there is a regularity result:

$$\|u\|_{H^s(\Gamma)} \leq C\|F\|_{H^{s+1}(\Gamma)} \quad \text{for } 0 \leq s < s_0$$

where s_0 is a positive number depending only on the angles of Γ . Applying this result with $s = 0$ to (58) rewritten as $V^*\varepsilon = F$, or in other words, $\Lambda\varepsilon = F - D^*\varepsilon$, we obtain that

$$\begin{aligned}\|\varepsilon\|_{L^2(\Gamma)} &\leq C(\|F\|_{H^1(\Gamma)} + \|D^*\varepsilon\|_{H^1(\Gamma)}) \\ &\leq C(\|F\|_{H^1(\Gamma)} + \|\varepsilon\|_{H^{-1/2}(\Gamma)})\end{aligned}$$

by the above mentioned continuity of D^* . Now by the unique solvability of (58), we also have the stability estimate $\|\varepsilon\|_{H^{-1/2}(\Gamma)} \leq C\|F\|_{H^1(\Gamma)}$. This, together with the continuous imbedding of $H^1(\Gamma)$ into $H^{1/2}(\Gamma)$ shows that

$$\|\varepsilon\|_{L^2(\Gamma)} \leq C\|F\|_{H^1(\Gamma)}. \quad (59)$$

We will use this regularity result in the proof of the next theorem.

Theorem 3. *There is an $H > 0$ and a $0 < \delta < 1$ such that whenever the coarse grid meshsize h_1 is less than H , the error reduction operator E of Algorithm 1 applied to the indefinite acoustic single layer equation satisfies*

$$\|\mathbf{E}\|_{\Lambda} \leq \delta. \quad (60)$$

Here, δ is independent of the refinement level J .

Proof. This proof proceeds by verifying (47) and applying Theorem 2. To verify (47), we begin with the following:

$$\begin{aligned}|\mathcal{D}(\sigma, \mu)| &= |\langle D\sigma, \mu \rangle| \leq \|D\sigma\|_{H^1(\Gamma)} \|\mu\|_{H^{-1}(\Gamma)} \\ &\leq C \|\sigma\|_{H^{-1/2}(\Gamma)} \|\mu\|_{H^{-1}(\Gamma)}.\end{aligned} \quad (61)$$

This is a consequence of Lemma 5. We shall use (61) several times below.

We first prove (47) for $k > 1$. Define $\tilde{D}_k = V_k P_k - \Lambda_k \tilde{P}_k$. Then $\langle \tilde{D}_k \sigma, \mu_k \rangle = \mathcal{D}(\sigma, \mu_k)$ for all σ in $H^{-1/2}(\Gamma)$ and all μ_k in M_k .

$$Z_k = T_k - \tilde{T}_k = R_k \left(V_k P_k - \Lambda_k \tilde{P}_k \right) = R_k \tilde{D}_k.$$

For any $\sigma \in \mathcal{M}_J$ and $k > 1$, we have

$$\begin{aligned}\|Z_k \sigma\|_{\Lambda}^2 &= \Lambda(R_k \tilde{D}_k \sigma, R_k \tilde{D}_k \sigma) \leq \tilde{\lambda}_k [R_k \tilde{D}_k \sigma, R_k \tilde{D}_k \sigma]_k && \text{by (31)} \\ &= \tilde{\lambda}_k \frac{1}{\tilde{\lambda}_k} (\tilde{D}_k \sigma, R_k \tilde{D}_k \sigma)_{-1} = \mathcal{D}(\sigma, R_k \tilde{D}_k \sigma) && \text{by (29)} \\ &\leq C \|\sigma\|_{H^{-1/2}(\Gamma)} \|R_k \tilde{D}_k \sigma\|_{H^{-1}(\Gamma)} && \text{by (61)}.\end{aligned}$$

The last factor can be estimated by

$$\begin{aligned}\|R_k \tilde{D}_k \sigma\|_{H^{-1}(\Gamma)}^2 &= (R_k \tilde{D}_k \sigma, R_k \tilde{D}_k \sigma)_{-1} \leq C [R_k \tilde{D}_k \sigma, R_k \tilde{D}_k \sigma]_k \\ &= C \frac{1}{\tilde{\lambda}_k} (\tilde{D}_k \sigma, R_k \tilde{D}_k \sigma)_{-1} \leq C \frac{1}{\tilde{\lambda}_k} \|\tilde{D}_k \sigma\|_{H^{-1}(\Gamma)} \|R_k \tilde{D}_k \sigma\|_{H^{-1}(\Gamma)},\end{aligned}$$

and also noting that

$$\begin{aligned}\|\tilde{D}_k\sigma\|_{-1}^2 &= (\tilde{D}_k\sigma, \tilde{D}_k\sigma)_{-1} = \left((V_k P_k - \Lambda_k \tilde{P}_k)\sigma, \tilde{D}_k\sigma \right)_{-1} \\ &= \mathcal{D}(\sigma, \tilde{D}_k\sigma) \leq C \|\sigma\|_{H^{-1/2}(\Gamma)} \|\tilde{D}_k\sigma\|_{H^{-1}(\Gamma)}.\end{aligned}$$

In combination, these show

$$\|Z_k\sigma\|_{\Lambda} = \|R_k \tilde{D}_k\sigma\|_{\Lambda} \leq C \tilde{\lambda}_k^{-1/2} \|\sigma\|_{H^{-1/2}(\Gamma)} \leq C h_k^{1/2} \|\sigma\|_{H^{-1/2}(\Gamma)}.$$

The last inequality follows from (31) and (38). Hence, for $k \geq 2$,

$$\|Z_k\| = \sup_{\sigma \in \mathcal{M}_k} \frac{\|Z_k\sigma\|_{\Lambda}}{\|\sigma\|_{\Lambda}} \leq C h_k^{1/2},$$

so we have verified (47) with $\alpha = 1/2$.

To prove (47) on the coarsest level ($k = 1$), we will use (59) and the following duality argument along the lines of a similar argument in [11]. Let σ in \mathcal{M}_k . Define

$$F(\eta) = (\eta, (I - P_1)\sigma)_{-1}.$$

This is a continuous linear functional on $H^{-1/2}(\Gamma)$ and hence there is a unique solution ε to (58) with this F . Hence,

$$\begin{aligned}\|(I - P_1)\sigma\|_{H^{-1}(\Gamma)}^2 &= \overline{F((I - P_1)\sigma)} \\ &= \mathcal{V}((I - P_1)\sigma, \varepsilon) \\ &= \mathcal{V}((I - P_1)\sigma, \varepsilon - \varepsilon_1) \\ &\leq C \|(I - P_1)\sigma\|_{H^{-1/2}(\Gamma)} \|\varepsilon - \varepsilon_1\|_{H^{-1/2}(\Gamma)}\end{aligned}\quad (62)$$

for any ε_1 in \mathcal{M}_1 . We choose an ε_1 with optimal approximation properties. Note that since

$$\|F\|_{H^1(\Gamma)} = \|(I - P_1)\sigma\|_{H^{-1}(\Gamma)},$$

the regularity result (59) holds for ε . Therefore,

$$\begin{aligned}\|\varepsilon - \varepsilon_1\|_{H^{-1/2}(\Gamma)} &\leq C h_1^{1/2} \|\varepsilon\|_{L^2(\Gamma)} \leq C h_1^{1/2} \|F\|_{H^1(\Gamma)} \\ &= C h_1^{1/2} \|(I - P_1)\sigma\|_{H^{-1}(\Gamma)}.\end{aligned}$$

Using this in (62), we conclude that

$$\|(I - P_1)\sigma\|_{H^{-1}(\Gamma)} \leq C h_1^{1/2} \|(I - P_1)\sigma\|_{H^{-1/2}(\Gamma)}. \quad (63)$$

We use (63) to estimate the norm of Z_1 as follows.

$$\begin{aligned}\Lambda(Z_1\sigma, \mu_1) &= \Lambda((P_1 - \tilde{P}_1)\sigma, \mu_1) = D((I - P_1)\sigma, \mu_1) \\ &\leq C \|(I - P_1)\sigma\|_{H^{-1}(\Gamma)} \|\mu_1\|_{\Lambda} && \text{by (61)} \\ &\leq C h_1^{1/2} \|(I - P_1)\sigma\|_{H^{-1/2}(\Gamma)} \|\mu_1\|_{\Lambda} && \text{by (63)} \\ &\leq C h_1^{1/2} \|\sigma\|_{H^{-1/2}(\Gamma)} \|\mu_1\|_{\Lambda} && \text{by Lemma 3.}\end{aligned}$$

This proves (47) for the $k = 1$ case as well.

Hence, we can apply Theorem 2 with $\alpha = 1/2$ to get

$$\|\mathbf{E}\|_{\Lambda} \leq \|\tilde{\mathbf{E}}\|_{\Lambda} + C_2 h_1^{1/2} \leq \tilde{\delta} + C_2 h_1^{1/2},$$

where $\tilde{\delta}$ is a positive number less than one given by Theorem 1. It is now clear that when h_1 is small enough, the result follows.

4 Numerical Experiments

4.1 Effect of weaker inner product on eigenfunctions

The performance of the multigrid algorithm described in Section 2 depends crucially on the spectral behavior of the positive definite operator Λ . For a discretized version of this integral operator the eigenfunctions corresponding to small magnitude eigenvalues are highly oscillatory, while those eigenfunctions corresponding to the large end of the spectrum are non-oscillatory. Standard multigrid approaches are successful for operator equations with the opposite spectral behavior and the use of the weaker inner products from Section 2.1 effectively transforms the single layer problem into this setting. In this section we present the details of two examples showing the undesirable behaviour of the discrete eigenfunctions of the stiffness matrix associated with Λ while working in the (natural) $H^{-1/2}(\Gamma)$ inner product, and the effect of working with the weaker inner product instead. We demonstrate the effectiveness of this approach for two geometries, a (smooth) circle and a Lipschitz domain (square).

Recall again that if the boundary Γ is discretized by means of a partition $x_1, x_2, \dots, x_N, x_{N+1} = x_1$, we denote by ϕ_i and l_i the characteristic function and respectively the length of the element $\tau_i = \text{conv}(x_i, x_{i+1})$. The span of the $\{\phi_i\}$ is denoted by \mathcal{M}_k . In the case of the square, the boundary discretization consists of straight line segments; whereas in the case of the circle our discretization consists of arcs of equal angle. The basis coefficients of an element $\sigma \in \mathcal{M}_k$ with respect to the $\{\phi_i\}$ are given in terms of the vector $\mathbf{e}(\sigma)$ defined in (10).

For a given discretization we are interested in the spectrum of the $N \times N$ stiffness matrix corresponding to the single layer operator for the Laplacian with entries $[\Lambda]_{i,j} = \langle \Lambda \phi_j, \phi_i \rangle$. In Figure 1 the left-hand plots show the eigenfunction of Λ for a circular domain, corresponding to the smallest (top left) and largest (bottom left) eigenvalues respectively. These figures illustrate the phenomenon described above.

In Section 2.1 we introduced a discrete inner product on the discretization space and proved that its associated norm is equivalent to the natural $H^{-1}(\Gamma)$ norm. As before we denote by \mathbf{A} the finite difference matrix corresponding to $-u'' + u$ on Γ with periodic boundary conditions, and by \mathbf{H} the diagonal matrix with i^{th} diagonal entry l_i . According to the definition of the discrete inner

product in (12) we find for $\sigma, \theta \in \mathcal{M}_k$:

$$\begin{aligned} [\sigma, \theta]_k &= \left\langle \sum_i [\mathbf{e}(A^{-1}\sigma)]_i \phi_i, \sum_j [\mathbf{e}(\theta)]_j \phi_j \right\rangle_\Gamma = \sum_i [\mathbf{e}(A^{-1}\sigma)]_i \overline{[\mathbf{e}(\theta)]_i} l_i \\ &= [\mathbf{e}(\theta)]^* \mathbf{H} \mathbf{A}^{-1} [\mathbf{e}(\sigma)], \end{aligned}$$

and also,

$$\Lambda(\theta, \theta) = \sum_{i,j} [\mathbf{e}(\theta)]_i \overline{[\mathbf{e}(\theta)]_j} \underbrace{\Lambda(\phi_i, \phi_j)}_{\Lambda_{j,i}} = [\mathbf{e}(\theta)]^* \Lambda [\mathbf{e}(\theta)].$$

The smoothing procedure, defined in Section 2.2, depends on the largest eigenvalue of the following Rayleigh quotient with respect to the weaker inner product.

$$\lambda = \sup_{\theta \in \mathcal{M}_k} \frac{\Lambda(\theta, \theta)}{[\theta, \theta]_k} = \sup_{\theta \in \mathcal{M}_k} \frac{\mathbf{e}(\theta)^* \Lambda \mathbf{e}(\theta)}{\mathbf{e}(\theta)^* \mathbf{H} \mathbf{A}^{-1} \mathbf{e}(\theta)} = \sup_{y \in \mathbb{R}^N} \frac{y^* \mathbf{A}^* \Lambda \mathbf{A} y}{y^* \mathbf{A}^* \mathbf{H} y}.$$

The two matrices $\mathbf{A}^* \Lambda \mathbf{A}$ and $\mathbf{A}^* \mathbf{H}$ are Hermitian. Therefore, λ is the largest generalized eigenvalue of the problem:

$$\mathbf{A}^* \Lambda \mathbf{A} y = \lambda \mathbf{A}^* \mathbf{H} y, \quad \text{or equivalently,} \quad \Lambda \mathbf{A} y = \lambda \mathbf{H} y. \quad (64)$$

The corresponding eigenfunction is given in terms of its basis coefficients $\mathbf{e}(\theta) = \mathbf{A} y$. We note that the L^2 norm of θ is easy to compute.

$$\|\theta\|_{L^2}^2 = \sum_{i,j} [\mathbf{e}(\theta)]_i \overline{[\mathbf{e}(\theta)]_j} \langle \phi_i, \phi_j \rangle = \mathbf{e}(\theta)^* \mathbf{H} \mathbf{e}(\theta) = y^* \mathbf{A}^* \mathbf{H} \mathbf{A} y.$$

This allows us to normalize the coefficient vector $\mathbf{e}(\theta)$ such that θ has norm one in $L^2(\Gamma)$. We are now ready to examine the spectral behavior in the smoothing operation in terms of the generalized eigenvalue problem (64).

In the case where Γ is a circle centered at the origin, the entries of the matrix Λ are particularly simple to compute. We require the radius to be bounded by $R < 1/2$ in order to guarantee the positive definiteness of the integral operator Λ and we discretize the circle with arcs Γ_i , $i = 1..N$ of equal angle.

$$\begin{aligned} [\Lambda]_{ij} &= \langle \Lambda \Phi_j, \Phi_i \rangle = -\frac{1}{2\pi} \int_{\Gamma_i} \int_{\Gamma_j} \log(|x-y|) ds_x ds_y \\ &= -\frac{1}{2\pi} \frac{1}{2} \int_{\Gamma_i} \int_{\Gamma_j} \log(2R^2(1 - \cos(\theta_i - \theta_j))) R^2 d\theta_j d\theta_i \\ &= -\frac{R^2}{4\pi} \int_{\Gamma_i} \int_{\Gamma_j} \log(2R^2) d\theta_j d\theta_i - \underbrace{\frac{R^2}{4\pi} \int_{\Gamma_i} \int_{\Gamma_j} \log(1 - \cos(\theta_i - \theta_j)) d\theta_j d\theta_i}_{I_{ji}} \\ &= -\frac{R^2}{4\pi} \log(2R^2) \left(\frac{2\pi}{N}\right)^2 - \frac{R^2}{4\pi} I_{ji} = -\frac{R^2}{4\pi} \left\{ \log(2R^2) \left(\frac{2\pi}{N}\right)^2 + I_{ji} \right\} \end{aligned} \quad (65)$$

Hence, we have to evaluate the weakly singular integrals

$$I_{ji} = \int_{\Gamma_i} \int_{\Gamma_j} \log(1 - \cos(\theta_i - \theta_j)) d\theta_j d\theta_i$$

for all possible choices of Γ_i and Γ_j . Due to symmetry of the circle, the single layer matrix is a symmetric Toeplitz matrix and hence it is sufficient to compute its first row. For $|i - j| > 1$, the integrand in I_{ij} is smooth, and we use Gaussian quadrature to compute the entries. In the two remaining cases when either $|i - j| = 1 \pmod N$ or $i = j$, we separate the singularity of the integrand according to

$$\begin{aligned} \log(1 - \cos(t)) &= \log\left(\frac{t^2}{2} - \frac{t^4}{4!} + \frac{t^6}{6!} - \frac{t^8}{8!} + \dots\right) \\ &= \underbrace{\log(t^2)}_{f_s} - \log(2) + \underbrace{\log\left(1 - \frac{2t^2}{4!} + \frac{2t^4}{6!} + \dots\right)}_{f_a} \quad (66) \\ &= f_s(t) + f_a(t). \end{aligned}$$

We then integrate the singular term $f_s(t)$ exactly and use Gaussian quadrature to compute the integral over the nonsingular function $f_a(t)$.

Figure 1 shows the effect of the smoothing operator. The eigenfunction of the generalized eigenvalue problem $\Lambda Ay = \lambda Hy$ corresponding to the smallest eigenvalue (top right) is smooth (and represents a function of period 2π on the circle). The eigenfunction of the largest eigenvalue (bottom right) is highly oscillatory. All eigenfunctions shown correspond to $N = 300$ elements on the circle.

As a second test case we consider a square with side length $1/2$. We compute the eigenfunctions corresponding to the four smallest and the four largest eigenvalues for both the stiffness matrix Λ and the generalized eigenvalue problem $\Lambda Ay = \lambda Hy$. Figures 2 and 3 illustrate the results for a uniform discretization of the boundary curve Γ with meshsize $h = 1/50$. Again, we observe that the eigenfunctions of the generalized eigenvalue problem display the reversed (and sought-after) smoothness behavior. The same behavior has been observed in cases of quasi-uniform meshes.

4.2 Multigrid convergence results

In this section we present numerical convergence results for the multigrid algorithm described in Section 2 to underline its effective use. Various results from a different set of experiments have already been reported in [13]. Recall that we want to solve the exterior Helmholtz problem with prescribed Dirichlet data on the boundary of a scattering object. The fundamental solution $i/4 H_0^{(1)}(\kappa \|x - x^*\|)$ solves the Helmholtz equation away from its singularity x^* and satisfies the correct growth condition at infinity. If we place the singularity into the interior of the scattering domain, we can use this so called point source

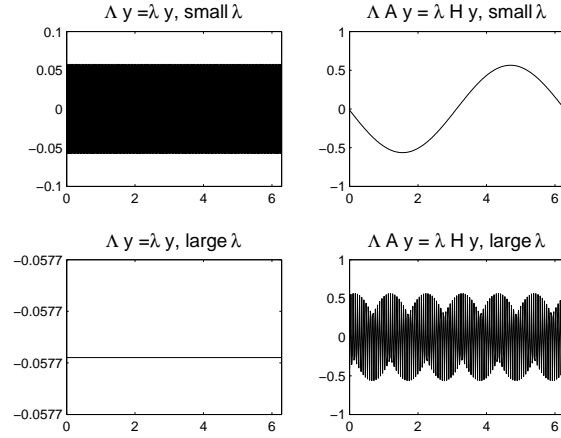


Figure 1: Eigenfunction behavior, circular curve
 Eigenfunctions for a circular curve with $N = 300$. They correspond to the smallest e-val of Λ (top left), the smallest e-val of $\Lambda A y = \lambda H y$ (top right), the largest e-val of Λ (bottom left) and the largest e-val of $\Lambda A y = \lambda H y$ (bottom right).

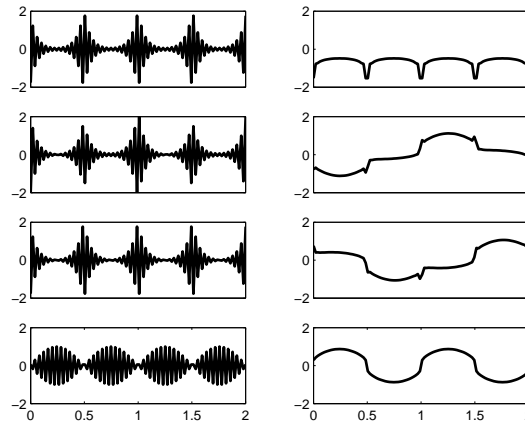


Figure 2: Eigenfunction behavior, square boundary curve, small eigenvalues
 Eigenfunction behavior for a square boundary curve Γ and a uniform mesh with mesh size $h = 1/50$. Eigenfunctions correspond to the four smallest e-vals of Λ (left) and the four smallest generalized e-vals of $\Lambda A y = \lambda H y$ (right).

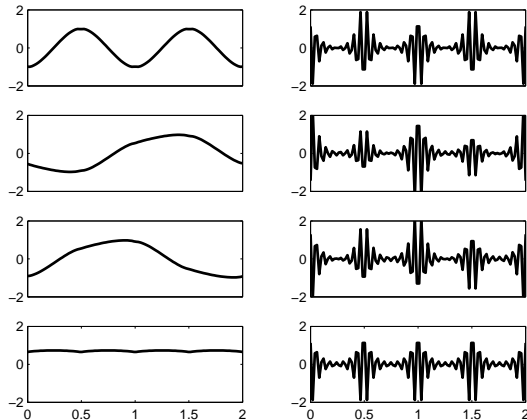


Figure 3: Eigenfunction behavior, square boundary curve, large eigenvalues
Eigenfunction behavior for a square boundary curve Γ and a uniform mesh with mesh size $h = 1/50$. Eigenfunctions correspond to the four largest e-vals of Λ (left) and the four largest generalized e-vals of $\Lambda Ay = \lambda Hy$ (right).

problem as a convenient test case, for which the exact solution is known. We also present results for the scattering of an incident plane wave by polygonal shaped obstacles. In all the tables below, \mathbf{H} is the coarsest mesh size, and \mathbf{h} is the finest mesh.

The fast implementation of the matrix-vector multiplications in the algorithm was not subject of our study and hence we do not report on the overall CPU time used by the algorithm. We anticipate that the CPU time will be competitive once those matrix operations are implemented using matrix-compression techniques such as H-matrices.

4.2.1 Effect of domain shape on performance

We first present results for point-source scattering from 4 different objects: a square, a rectangle (sides of ratio 1:4), an equilateral triangle and a thin wedge. The thin wedge is described in terms of the xy-coordinates of its three corner points, namely $(0, 0)$, $(1/3, \sqrt{3}/3)$ and $(0, 1/15)$. This amount to an angle of $\pi/3$ between the horizontal x-axis and the lower edge of the wedge. In each of these examples, the diameter of the object is less than 1, which guarantees the positive definiteness of the potential single layer operator in the sense of (4). In each of Tables 1-4, the proposed multigrid scheme is used as a linear solver. We report the number of iteration numbers required to reach a given relative residual norm. The point source is located inside the domain, so the true solution is known in each case.

Table 1: Linear multigrid iteration counts with $\kappa = 2.1$, point-source inside square, 10^{-6} relative residual norm

| | H | | | | | Degrees of freedom |
|---------------|----------|-----|-----|------|------|-----------------------|
| | 1/2 | 1/4 | 1/8 | 1/16 | 1/32 | |
| 1/4 | 17 | - | - | - | - | 32 |
| 1/8 | 16 | 15 | - | - | - | 64 |
| 1/16 | 15 | 15 | 15 | - | - | 128 |
| h 1/32 | 15 | 15 | 15 | 15 | - | 256 |
| 1/64 | 16 | 16 | 15 | 15 | 15 | 512 |
| 1/128 | 16 | 16 | 16 | 16 | 16 | 1024 |
| 1/256 | 16 | 16 | 16 | 16 | 16 | 2048 |

Table 2: Linear multigrid iteration counts with $\kappa = 2.1$, point-source inside rectangle, 10^{-6} relative residual norm

| | H | | | | | Degrees of freedom |
|---------------|----------|-----|-----|------|------|-----------------------|
| | 1/2 | 1/4 | 1/8 | 1/16 | 1/32 | |
| 1/4 | 15 | - | - | - | - | 72 |
| 1/8 | 17 | 15 | - | - | - | 144 |
| 1/16 | 18 | 18 | 16 | - | - | 288 |
| h 1/32 | 18 | 19 | 18 | 16 | - | 576 |
| 1/64 | 19 | 19 | 19 | 18 | 16 | 1152 |
| 1/128 | 19 | 19 | 19 | 19 | 19 | 2304 |

Table 3: Linear multigrid iteration counts with $\kappa = 2.1$, point-source inside triangle, 10^{-6} relative residual norm

| | H | | | | | | | | Degr. of freedom |
|---------------|----------|-----|-----|-----|------|------|------|-------|---------------------|
| | 1 | 1/2 | 1/4 | 1/8 | 1/16 | 1/32 | 1/64 | 1/128 | |
| 1/2 | 21 | - | - | - | - | - | - | - | 6 |
| 1/4 | 33 | 30 | - | - | - | - | - | - | 12 |
| 1/8 | 37 | 37 | 36 | - | - | - | - | - | 24 |
| 1/16 | 28 | 28 | 27 | 27 | - | - | - | - | 48 |
| h 1/32 | 24 | 24 | 24 | 23 | 23 | - | - | - | 96 |
| 1/64 | 23 | 23 | 23 | 22 | 22 | 22 | - | - | 192 |
| 1/128 | 22 | 22 | 22 | 22 | 22 | 21 | 22 | - | 384 |
| 1/256 | 21 | 21 | 21 | 21 | 21 | 21 | 21 | 21 | 768 |
| 1/512 | 20 | 20 | 20 | 21 | 21 | 21 | 20 | 20 | 1536 |

Table 4: Linear multigrid iteration counts with $\kappa = 2\pi$, thin wedge, pre-smoothing only, 10^{-4} relative residual norm

| | | H | | | | | Degr. of freedom |
|----------|-------|----------|-----|------|------|------|------------------|
| | | 1/4 | 1/8 | 1/16 | 1/32 | 1/64 | |
| h | 1/16 | 31 | 21 | - | - | - | 352 |
| | 1/32 | 18 | 13 | 9 | - | - | 704 |
| | 1/64 | 17 | 11 | 8 | 5 | - | 1408 |
| | 1/128 | 17 | 11 | 7 | 4 | 3 | 2816 |

Table 5: Linear multigrid iteration counts with $\kappa = 10.2$, point source inside triangle, pre-smoothing only, 10^{-6} relative residual norm

| | | H | | | | | Degr. of freedom | |
|----------|-------|----------|-----|------|------|------|------------------|------|
| | | 1/4 | 1/8 | 1/16 | 1/32 | 1/64 | 1/128 | |
| h | 1/8 | 38 | - | - | - | - | - | 24 |
| | 1/16 | 36 | 33 | - | - | - | - | 48 |
| | 1/32 | 32 | 30 | 28 | - | - | - | 96 |
| | 1/64 | 27 | 26 | 25 | 24 | - | - | 192 |
| | 1/128 | 24 | 23 | 22 | 22 | 22 | - | 384 |
| | 1/256 | 22 | 21 | 21 | 21 | 21 | 22 | 768 |
| | 1/512 | 21 | 21 | 21 | 21 | 21 | 21 | 1536 |

4.2.2 Multigrid as linear solver/ preconditioner

In this section, we provide results about the use of the proposed multigrid scheme as a linear solver (Tables ??), and as a preconditioner for GMRES (used without restart, Tables ??). We present iteration counts in each case with just pre-smoothing, or with both pre-and post-smoothing. We use the same equilateral triangle as the domain as in the previous section. Again, a point-source is placed inside the domain, so we can compare with the exact solution. In contrast to the previous section, here we present results for wave number $\kappa = 10.2$. The tolerances in relative residual norm are 10^{-6} , 10^{-9} for the linear solver and preconditioned GMRES, respectively. For both, multigrid as a linear solver and preconditioned GMRES, the iteration numbers stay almost constant with increasing degree of freedom, whereas the iteration numbers of GMRES grow considerably. Convergence for the algorithm with an additional postsmoothing step follows from our convergence result by standard arguments in multigrid theory.

4.2.3 Effect of frequency on performance

Here we present the effect of increasing κ on the number of multigrid iterations taken to achieve a given relative residual error. We place a point source inside a square whose diameter is less than 1. We expect the coarsest mesh required should satisfy the constraint $\kappa\mathbf{H} \approx \text{constant}$. At least in this example, the

Table 6: Linear multigrid iteration counts with $\kappa = 10.2$, point source inside triangle, pre- and post-smoothing, 10^{-6} relative residual norm

| | H | | | | | | Degr. of freedom |
|---------------|----------|-----|------|------|------|-------|------------------|
| | 1/4 | 1/8 | 1/16 | 1/32 | 1/64 | 1/128 | |
| 1/8 | 19 | - | - | - | - | - | 24 |
| 1/16 | 20 | 17 | - | - | - | - | 48 |
| h 1/32 | 18 | 16 | 14 | - | - | - | 96 |
| 1/64 | 17 | 15 | 14 | 13 | - | - | 192 |
| 1/128 | 15 | 14 | 13 | 13 | 13 | - | 384 |
| 1/256 | 15 | 13 | 13 | 13 | 13 | 13 | 768 |
| 1/512 | 16 | 14 | 13 | 13 | 13 | 13 | 1536 |

Table 7: GMRES iteration counts, $\kappa = 10.2$, point source inside triangle, triangle, pre-smoothing only, 10^{-9} relative residual norm

| | H | | | | GMRES | |
|---------------|----------|-----|-----|------|-------------------------|--|
| | 1/2 | 1/4 | 1/8 | 1/16 | without preconditioning | |
| 1/8 | 17 | 16 | - | - | 16 | |
| 1/16 | 23 | 21 | 20 | - | 24 | |
| h 1/32 | 23 | 22 | 22 | 19 | 31 | |
| 1/64 | 24 | 23 | 23 | 22 | 37 | |
| 1/128 | 25 | 25 | 24 | 23 | 44 | |
| 1/256 | 25 | 27 | 24 | 23 | 52 | |
| 1/512 | 26 | 28 | 24 | 24 | 63 | |
| 1/1024 | 27 | 28 | 26 | 26 | 74 | |

Table 8: GMRES iteration counts, $\kappa = 10.2$, triangle, uniform grid, $\theta = 1$, pre and post-smoothing, 10^{-9} relative residual norm

| | H | | | | GMRES | |
|---------------|----------|-----|-----|------|-------------------------|--|
| | 1/2 | 1/4 | 1/8 | 1/16 | without preconditioning | |
| 1/8 | 18 | 15 | - | - | 16 | |
| 1/16 | 20 | 17 | 17 | - | 242 | |
| h 1/32 | 20 | 18 | 18 | 17 | 31 | |
| 1/64 | 21 | 19 | 19 | 18 | 37 | |
| 1/128 | 21 | 21 | 19 | 19 | 44 | |
| 1/256 | 22 | 22 | 21 | 20 | 52 | |
| 1/512 | 22 | 24 | 21 | 21 | 63 | |
| 1/1024 | 23 | 24 | 21 | 21 | 74 | |

Table 9: Linear multigrid iteration counts with $\kappa = 2.1$, point source inside square, pre- and post-smoothing, 10^{-6} relative residual norm

| | | H | | | | | | | Degr. of freedom |
|----------|-------|----------|-----|------|------|------|-------|-------|------------------|
| | | 1/4 | 1/8 | 1/16 | 1/32 | 1/64 | 1/128 | 1/256 | |
| h | 1/32 | 12 | 12 | 12 | - | - | - | - | 256 |
| | 1/64 | 13 | 13 | 12 | 12 | - | - | - | 512 |
| | 1/128 | 13 | 13 | 13 | 13 | 12 | - | - | 1024 |
| | 1/256 | 13 | 13 | 13 | 13 | 13 | 13 | - | 2048 |
| | 1/512 | 14 | 14 | 14 | 14 | 14 | 13 | 13 | 4096 |

Table 10: Linear multigrid iteration counts with $\kappa = 10.2$, point source inside square, pre- and post-smoothing, 10^{-6} relative residual norm. The method did not converge for $\mathbf{H}=1/4$.

| | | H | | | | | | | Degr. of freedom |
|----------|-------|----------|-----|------|------|------|-------|-------|------------------|
| | | 1/4 | 1/8 | 1/16 | 1/32 | 1/64 | 1/128 | 1/256 | |
| h | 1/32 | * | 15 | 13 | - | - | - | - | 256 |
| | 1/64 | * | 14 | 12 | 11 | - | - | - | 512 |
| | 1/128 | * | 14 | 12 | 11 | 11 | - | - | 1024 |
| | 1/256 | * | 13 | 12 | 11 | 11 | 11 | - | 2048 |
| | 1/512 | * | 12 | 12 | 12 | 12 | 12 | 12 | 4096 |

method performs well even though this constraint was not strictly satisfied. For example, in Table 9, $\kappa H = 0.252$, while in Table 11, $\kappa H = 1.575$,

The numerical experiments show that the multigrid algorithm presented and analyzed in this paper is an efficient tool to solve the first kind single layer equation when used as a linear solver or as a preconditioning procedure for other solvers such as GMRES.

Table 11: Linear multigrid iteration counts with $\kappa = 50.4$, point source inside square, pre- and post-smoothing, 10^{-6} relative residual norm. The method did not converge for $\mathbf{H} > 1/32$.

| | | H | | | | | | | Degr. of freedom |
|----------|-------|----------|-----|------|------|------|-------|-------|------------------|
| | | 1/4 | 1/8 | 1/16 | 1/32 | 1/64 | 1/128 | 1/256 | |
| h | 1/32 | * | * | * | * | - | - | - | 256 |
| | 1/64 | * | * | * | * | - | - | - | 512 |
| | 1/128 | * | * | * | * | 13 | - | - | 1024 |
| | 1/256 | * | * | * | * | 13 | 11 | - | 2048 |
| | 1/512 | * | * | * | * | 12 | 11 | 11 | 4096 |

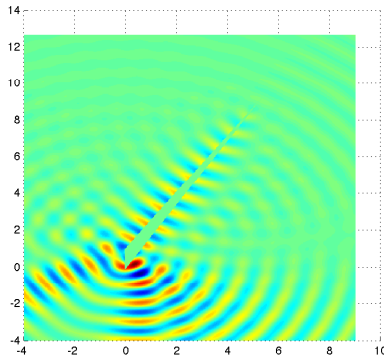


Figure 4: Plane-wave scattering from wedge: linear MG is used to compute the unknown density, and numerical quadrature is used to reconstruct the scattered field.

References

- [1] H. Brakhage and P. Werner. Über das Dirichletsche Aussenraumproblem für die Helmholtzsche Schwingungsgleichung. *Arch. Math.*, 16:325329, 1965.
- [2] J. H. Bramble. *Multigrid methods*, volume 294 of *Pitman Research Notes in Mathematics Series*. Longman Scientific & Technical, 1993.
- [3] J. H. Bramble, D. Y. Kwak, and Joseph E. Pasciak. Uniform convergence of multigrid V -cycle iterations for indefinite and nonsymmetric problems. *SIAM J. Numer. Anal.*, 31(6):1746–1763, 1994.
- [4] J. H. Bramble, Z. Leyk, and J. E. Pasciak. The analysis of multigrid algorithms for pseudodifferential operators of order minus one. *Math. Comp.*, 63(208):461–478, 1994.
- [5] J. H. Bramble and J. E. Pasciak. New estimates for multilevel algorithms including the V -cycle. *Math. Comp.*, 60(202):447–471, 1993.
- [6] J. H. Bramble, J. E. Pasciak, and O. Steinbach. On the stability of the L^2 projection in $H^1(\Omega)$. *Math. Comp.*, 71(237):147–156, 2002.
- [7] S. Chandler-Wilde and I. Graham. Boundary integral methods in high frequency scattering. In *B. Engquist, A. Fokas, E. Hairer, and A. Iserles, editors, highly oscillatory problems*. Cambridge University Press, 2009
- [8] S.N. Chandler-Wilde, I.G. Graham, S. Langdon, and M. Lindner. Condition number estimates for combined potential boundary integral operators in acoustic scattering. *Journal of Integral Equations and Applications*, 21:229279, 2009.

- [9] S.N. Chandler-Wilde and S. Langdon. A wavenumber independent BEM for an acoustic scattering problem. *SIAM J. Numer. Anal.*, 46:24502477, 2006.
- [10] S.N. Chandler-Wilde and P. Monk. Wave-number-explicit bounds in time-harmonic scattering. *SIAM J. Math. Anal.*, 39:14281455, 2008.
- [11] M. Costabel and E. P. Stephan. Duality estimates for the numerical solution of integral equations. *Numer. Math.*, 54(3):339–353, 1988.
- [12] S.A. Funken and E.P. Stephan. The BPX preconditioner for the single layer potential operator. *Appl. Anal.*, 67(3-4):327–340, 1997.
- [13] S. Gemmrich, J. Gopalakrishnan, and N. Nigam. The performance of a multigrid algorithm for the acoustic single layer equation. In *Numerical Mathematics and Advanced Applications: Proceedings of ENUMATH 2007, the 7th European Conference on Numerical Mathematics and Advanced Applications*, pages 175–182. Springer, Heidelberg, 2008.
- [14] J. Gopalakrishnan, J. E. Pasciak, and L. F. Demkowicz. Analysis of a multigrid algorithm for time harmonic Maxwell equations. *SIAM J. Numer. Anal.*, 42(1):90–108 (electronic), 2004.
- [15] G.C. Hsiao, E.P. Stephan, and W.L. Wendland. On the Dirichlet problem in elasticity for a domain exterior to an arc. *J. Comput. Appl. Math.*, 34(1):1–19, 1991.
- [16] G.C. Hsiao and W.L. Wendland. *Boundary integral equations*, volume 164 of *Applied Mathematical Sciences*. Springer-Verlag, Berlin, 2008.
- [17] George Hsiao and R. C. MacCamy. Solution of boundary value problems by integral equations of the first kind. *SIAM Rev.*, 15:687–705, 1973.
- [18] U. Langer, D. Pusch, and S. Reitzinger. Efficient preconditioners for boundary element matrices based on grey-box algebraic multigrid methods. *Internat. J. Numer. Methods Engrg.*, 58(13):1937–1953, 2003.
- [19] U. Langer and U. Pusch. Convergence analysis of geometrical multigrid methods for solving data-sparse boundary element equations. In *Proc. 8th European Multigrid Conference 2005*. Springer, Heidelberg, 2007.
- [20] M. Löhndorf and J.M. Melenk. Wavenumber-explicit hp-BEM for high frequency scattering. To appear in *SIAM J. Numer. Anal.*, preprint <http://www.asc.tuwien.ac.at/preprint/2010/asc02x2010.pdf>
- [21] M. Maischak, P. Mund, and E. P. Stephan. Adaptive multilevel BEM for acoustic scattering. *Comput. Methods Appl. Mech. Engrg.*, 150(1-4):351–367, 1997.

- [22] J.M. Melenk and S.Sauter Wavenumber explicit convergence analysis for Galerkin discretizations of the Helmholtz equation *SIAM J. Numer. Anal.* 49 (2011), pp. 1210–1243
- [23] S. Sauter and C. Schwab. *Randelementmethoden, Analyse, Numerik und Implementierung schneller Algorithmen.* Teubner, 2004.
- [24] O. Steinbach. *Numerische Näherungsverfahren für elliptische Randwertprobleme.* Teubner, Stuttgart, Leipzig, Wiesbaden, 2003.